

All the Disorder Mechanisms in the 13:58 Phases Come Together. Out of the Modulated Confusion Rises the Remarkable Phase $\text{Ce}_{12.60}\text{Cd}_{58.68(2)}$

Shu Ying Piao,[†] Lukas Palatinus,^{‡§} and Sven Lidin^{*†}

Inorganic Chemistry, Arrhenius Laboratory, Stockholm University, S-106 91 Stockholm, Sweden, and Ecole Polytechnique Fédérale de Lausanne, 1015 Lausanne, Switzerland

Received October 4, 2007

The compound $\text{Ce}_{12.60}\text{Cd}_{58.68(2)}$ is a metrically commensurate representative of the incommensurately modulated phase $\text{Ce}_{13}\text{Cd}_{57+\delta}$. It is most likely a lock-in phase. The structure, which was solved using seeding of the modulation from those positions most affected as well as direct solution by charge flipping, represents a rare case of ordering in a family of structures where disorder is the rule. The disorder mechanisms, known from other $\text{RE}_{13}\text{Zn}/\text{Cd}_{58}$ phases, order in this phase to give rise to a remarkable interplay between interstitials and vacancies. The compound crystallizes in the super space group $Ccmm(\alpha 00)00s$ (standard setting $Amma(00\gamma)s00$) with cell parameters $a = 27.2789(14)$ Å, $b = 15.7592(1)$ Å, and $c = 15.5816(4)$ Å and a \mathbf{q} vector close to $2/3$.

Introduction

Many rare earth–zinc and rare earth–cadmium systems (RE–Zn/Cd) contain phases with a composition close to 1:6.^{1–9} These are isostructural with the 1:1 cubic approximants to the stable, icosahedral quasicrystals found in the systems Ca–Cd^{10,11} and Yb–Cd.¹² A higher, cubic approximant has been found both in some binary and in some ternary systems.^{13–15} Interestingly, many of the systems contain a

Table 1. Crystal Data, Data Collection, and Refinement Parameters for the Structures

Crystal data	
chemical formula	$\text{Ce}_{12.60}\text{Cd}_{58.68(2)}$
fw (g/mol)	8362
temp of measurement (K)	293
super space group	$Ccmm(\alpha 00)00s$
a (Å)	27.2789(14)
b (Å)	15.7592(1)
c (Å)	15.5816(4)
modulation wave vector \mathbf{q}	$2/3 a^*$
Z	4
cell volume (Å ³)	6698.4(4)
$F(000)$	14190
calcd density (g/cm ³)	8.29
abs coeff (mm ⁻¹)	26.503
$T_{\text{min}}, T_{\text{max}}$	0.35, 1.26
Data collection	
diffractometer	Xcalibur CCD diffractometer
range of 2θ (deg)	6.78–59.52
no. of measured reflns	49510
no. of independent reflns	19149
no. of obsd reflns	10494
no. of obsd main reflns	5008
no. of obsd satellites	5486
R_{int} (obsd/all) (%)	2.34/2.69
Refinement (on F)	
R_{all} (R, wR) (%)	5.54, 5.74
R_{main} (R, wR) (%)	3.74, 4.14
$R_{\text{satellite}}$ (R, wR), first order (%)	9.54, 9.11
no. of parameters	404
$\Delta\rho_{\text{max}}, \Delta\rho_{\text{min}}$ (e/Å ³)	5.67, –4.89
abs correction	numerical from shape

* To whom correspondence should be addressed. E-mail: sven@inorg.su.se.

[†] Stockholm University.

[‡] Ecole Polytechnique Fédérale de Lausanne.

[§] Permanent address: Institute of Physics of the ASCR, v. v. i., Na Slovance 2, 182 21 Prague, Czech Republic.

- (1) Bruzzone, G.; Fornazini, M. L.; Merlo, F. *J. Less-Common Met.* **1973**, *30*, 361.
- (2) Wang, F. E. *Acta Crystallogr.* **1967**, *22*, 579.
- (3) Larson, A. C.; Cromer, D. T. *Acta Crystallogr., Sect. B: Struct. Sci.* **1971**, *27*, 1875.
- (4) Palenzona, A. *J. Less-Common Met.* **1971**, *25*, 367.
- (5) Sands, D. E.; Johnson, Q. C.; Krikorian, O. H.; Kromholtz, K. L. *Acta Crystallogr.* **1962**, *15*, 1191.
- (6) Armbruster, M.; Lidin, S. *J. Alloys Compd.* **2000**, *307*, 141.
- (7) Gomez, C. P.; Lidin, S. *Chem.—Eur. J.* **2004**, *10*, 3279.
- (8) Gomez, C. P.; Lidin, S. *Phys. Rev. B: Condens. Matter Mater. Phys.* **2003**, *68*, 24203.
- (9) Piao, S.; Gomez, C. P.; Lidin, S. *Z. Naturforsch., B: Chem. Sci.* **2006**, *60*, 644.
- (10) Tsai, A. P.; Guo, J. Q.; Abe, E.; Takakura, H.; Sato, T. *J. Nature (London, U.K.)* **2000**, *408*, 537.
- (11) Takakura, H.; Gomez, C. P.; Yamamoto, A.; Boissieu, M. D.; Tsai, A. P. *Nat. Mater.* **2006**, *6*, 58.
- (12) Guo, J. Q.; Abe, E.; Tsai, A. P. *Phys. Rev. B: Condens. Matter Mater. Phys.* **2000**, *62*, 14605.
- (13) Gomez, C. P.; Lidin, S. *Angew. Chem.* **2001**, *113*, 4161.
- (14) Lin, Q. S.; Corbett, J. D. *J. Am. Chem. Soc.* **2006**, *128*, 13268.

- (15) Lin, Q. S.; Corbett, J. D. *Proc. Natl. Acad. Sci. U.S.A.* **2006**, *103*, 13589.

Table 2. Fractional Atomic Coordinates and Isotropic ADPs for Ce_{12.60}Cd_{58.68}

element	atom	Wyck.	x	y	z	$U_{\text{iso}}/U_{\text{eq}}$ (Å ²)
Ce	Ce1a	8g	-0.02061(3)	0.43447(5)	-1/4	0.0137(3)
Ce	Ce1b	4c	0.29458(4)	-1/4	-1/4	0.0124(4)
Ce	Ce2a	16h	0.14714(2)	-0.06154(3)	-0.05258(4)	0.0119(2)
Ce	Ce2b	8f	0.45511(3)	1/4	-0.05447(6)	0.0116(2)
Ce	Ce3a	8g	-0.18734(4)	-0.06062(6)	-1/4	0.0206(6)
Ce	Ce3b	8f	0.6267(3)	-1/4	-0.2821(6)	0.0179(5)
Ce	Ce4	4b	1/4	1/4	0	0.0142(6)
Cd	Cd1a	16h	0.56620(4)	0.90216(6)	-0.09580(7)	0.0205(4)
Cd	Cd1b	16h	0.26811(4)	-0.0861(2)	-0.10207(1)	0.0390(6)
Cd	Cd1c	16h	0.0726(4)	0.4636(7)	0.090(1)	0.0277(8)
Cd	Cd1c2	16h	0.0889(2)	0.4471(3)	0.1017(4)	0.0213(5)
Cd	Cd2	4c	0.08202(6)	3/4	-0.75	0.0181(5)
Cd	Cd3	8f	0.08248(4)	3/4	-0.09481(8)	0.0146(3)
Cd	Cd4a	16h	0.20114(4)	0.10194(5)	-0.15644(7)	0.0254(3)
Cd	Cd4b	8f	0.34777(5)	1/4	-0.15864(9)	0.0220(5)
Cd	Cd5a	16h	0.1551(1)	0.3457(2)	-0.0008(3)	0.0244(5)
Cd	Cd5a2	16h	0.1654(5)	0.3854(9)	0.058(1)	0.050(1)
Cd	Cd5b	16h	0.2587(3)	0.0540(5)	0.0251(7)	0.0292(6)
Cd	Cd6a	8g	0.20899(4)	-0.07506(7)	-1/4	0.0162(3)
Cd	Cd6b	8g	0.43161(4)	0.35502(7)	-1/4	0.0193(4)
Cd	Cd6c	8g	0.39263(4)	0.47136(6)	1/4	0.0180(3)
Cd	Cd7a	16h	0.03052(3)	-0.40872(5)	-0.14002(6)	0.0172(2)
Cd	Cd7b	8f	0.68816(4)	1/4	-0.14441(8)	0.0154(3)
Cd	Cd8a	16h	-0.04765(3)	0.35230(5)	-0.05012(6)	0.0214(3)
Cd	Cd8b	8f	0.35230(5)	-1/4	-0.05273(8)	0.0182(4)
Cd	Cd9a	16h	-0.13135(3)	0.10111(5)	-0.15821(5)	0.0144(2)
Cd	Cd9b	8f	0.51721(4)	-1/4	-0.15800(7)	0.0141(3)
Cd	Cd10a	8g	0.11416(4)	-0.15268(6)	-1/4	0.0153(3)
Cd	Cd10b	4c	0.48241(7)	0.75	1/4	0.0156(5)
Cd	Cd11	4c	0.24931(7)	1/4	-1/4	0.0334(9)
Cd	Cd12a	8d	1/2	0	0	0.0390(9)
Cd	Cd12b	4a	1/4	3/4	0	0.041(1)
Cd	Cd13	8f	0.2498(1)	1/4	-0.0914(2)	0.0268(9)
Cd	Cd14	8f	0.8676(1)	3/4	0.0811(2)	0.068(2)

second phase with an approximate composition RE₁₃(Zn/Cd)₅₈.^{2,3,16–19} Although the basic structure of these phases is hexagonal, and thus cannot be claimed to be simple mathematical approximants to the icosahedral quasicrystals, the local arrangements are very similar to those in the RE₁₃(Zn/Cd)₆ phases, and the phases may be labeled as chemical approximants. Indeed, the structure of the archetype phase of RE₁₃Zn₅₈ may be described as a chemical twin of the 1:6 phase.¹⁹ A closer study of the RE₁₃Zn₅₈ phases has revealed that their structures are rather more complex than previously reported¹⁹ and that some of the disorder typical for the cubic approximants is also present in the (pseudo-)hexagonal cases. A very special case is that of Ce_{12.60}Cd_{58.68}(2).

The first report about Ce₁₃Cd_{~58} appeared in a remarkable paper by Roof and Elliot.²⁰ Their study showed that the compound has a variable composition and that the variation is manifested in a continuously changing superstructure. The authors describe this behavior as a bundle of microphases, a very reasonable approach before the idea of incommensurately modulated phases became widespread. The paper is particularly valuable since precession photographs of the hexagonal *h0l* zone from several different compositions are shown, and the behavior of the satellites is clear. There is

hence no doubt about the incommensurately modulated nature of the compound, although local lock-in phases are still permissible. The purpose of the present study was to determine the cause of the modulated behavior and, if possible, the details of the modulated structure.

Experimental Procedures

Synthesis and Characterization. Ce metal (chips, STREM 99.9%) and Cd metal (splinters from a Cd rod, CHEMPUR 99.9%) were mixed (0.2152 g/0.7702 g) inside a stainless steel tube, and the tube was sealed under an argon atmosphere. The tube was heated to 1033 K for 48 h in a muffle furnace. After annealing, the furnace was turned off with the sample left inside to cool to ambient temperature at a cooling rate of 3 K/min. The product was crystalline, silvery, and brittle. No secondary phase was detected by X-ray powder diffraction, although the slight imbalance between the nominal composition and the refined composition of the product indicates the presence of a more Ce-rich phase. Another possibility is a bifurcation of the 13:58 phase. If the compound presented in this study is indeed a lock-in phase, this indicates that other compositions, distinct from but arbitrarily close to that of Ce_{12.60}Cd_{58.68}, may exist in equilibrium. If, on the other hand, the phase is part of a continuous, incommensurate phase field, an equilibrium product should be a single phase with the same modulation **q** vector throughout the sample. It is impossible to determine as to which of these two cases is realized here. Synthetic procedures with slightly different starting compositions yielded crystals with different **q** vectors, exactly as reported by previously.²⁰ Irregularly shaped single crystals could easily be isolated from the resulting sample. The absence of impurities arising from reactions with the stainless steel ampule in the synthesized product was confirmed

(16) Bruzzone, G.; Fornasini, M. L.; Merlo, F. *J. Less-Common Met.* **1970**, *22*, 253.

(17) Bruzzone, G.; Fornasini, M. L.; Merlo, F. *J. Less-Common Met.* **1974**, *37*, 289.

(18) Gomes, C. P.; Lidin, S. *Solid State Sci.* **2002**, *4*, 901.

(19) Piao, S. Y.; Gomez, C. P.; Lidin, S. Z. *Kristallogr.—New Cryst. Struct.* **2006**, *221*, 391.

(20) Roof, R. B.; Elliot, R. B. *Inorg. Chem.* **1965**, *4*, 691.

Table 3. Positional Modulation^a

atom	modulation	Cxn	Cyn	Czn	Sxn	Syn	Szn
Ce1a	$n = 1$	0	0	0.0068(1)	0	0	-0.0025(1)
Ce1b	$n = 1$	0	0	-0.0015(2)	0	0	0.0102(2)
	$n = 2$	0.0013(2)	0	0	-0.0015(2)	0	0
Ce2a	$n = 1$	-0.00060(4)	0.00356(6)	0.00043(8)	-0.00072(4)	0.00199(7)	-0.00038(8)
Ce2b	$n = 1$	0.00005(6)	0	0.0030(1)	-0.00015(6)	0	-0.0012(1)
Ce3b	$n = 1$	-0.0015(2)	0	0.0043(6)	0.0008(3)	0	0.0051(9)
Ce4	$n = 1$	0	0	0	0.0073(1)	0	-0.0002(3)
Cd1a	$n = 1$	0.00311(6)	-0.00630(9)	-0.0050(1)	-0.00371(7)	0.0030(1)	-0.0007(1)
	$n = 2$	-0.0041(3)	0.0070(3)	0.0021(4)	-0.0041(1)	0.0057(3)	0.0036(4)
Cd1c	$n = 1$	0.0043(6)	0.0030(9)	0.003(2)	0.0019(3)	0.0014(5)	-0.0013(7)
Cd1c2	$n = 1$	-0.0024(3)	0.0016(5)	-0.0009(6)	-0.0049(2)	0.0048(3)	-0.0048(3)
Cd2	$n = 1$	0	0	0.0020(2)	0	0	0.0016(2)
Cd3	$n = 1$	0.00127(7)	0	-0.0007(2)	0.00085(7)	0	-0.0006(2)
Cd4a	$n = 1$	0.00216(7)	-0.0040(1)	-0.0042(1)	0.01059(6)	-0.00721(9)	0.0054(1)
Cd4b	$n = 1$	0.00192(8)	0	-0.0007(2)	0.00143(8)	0	-0.0102(2)
	$n = 2$	0.0039(2)	0	-0.0008(5)	0.0010(2)	0	0.0007(5)
Cd5a	$n = 1$	0.0023(1)	-0.0019(3)	0.0001(3)	-0.0059(2)	0.0023(3)	-0.0078(4)
Cd5a2	$n = 1$	0.0046(4)	-0.0038(8)	0.008(1)	0.0026(6)	-0.002(1)	0.006(2)
Cd5b	$n = 1$	-0.0014(2)	0.0048(2)	0.0014(2)	0.0023(5)	0.0016(7)	0.000(1)
Cd6a	$n = 1$	0	0	-0.0013(2)	0	0	-0.0027(2)
Cd6b	$n = 1$	0	0	-0.0055(2)	0	0	-0.0019(2)
Cd6c	$n = 1$	0	0	0.0037(2)	0	0	0.0008(2)
Cd7a	$n = 1$	0.00008(6)	0.00426(9)	-0.0040(1)	0.00003(5)	-0.00006(8)	-0.0003(1)
Cd7b	$n = 1$	-0.00093(7)	0	0.0004(2)	-0.00125(8)	0	-0.0018(2)
Cd8a	$n = 1$	-0.00386(6)	-0.00511(9)	0.0007(1)	0.00103(6)	0.0038(1)	-0.0000(1)
Cd8b	$n = 1$	-0.00448(9)	0	0.0034(2)	0.00836(9)	0	-0.0051(2)
	$n = 2$	-0.0000(2)	0	0.0001(4)	-0.0027(2)	0	0.0014(4)
Cd9a	$n = 1$	-0.00074(5)	0.00383(9)	-0.0000(1)	-0.00026(5)	-0.00491(8)	-0.0010(1)
Cd9b	$n = 1$	-0.00423(8)	0	0.0001(1)	-0.00240(8)	0	0.0010(2)
	$n = 2$	0.0007(2)	0	-0.0001(6)	0.0005(2)	0	-0.0011(6)
Cd10a	$n = 1$	0	0	-0.0008(2)	0	0	-0.0014(2)
Cd10b	$n = 1$	0	0	0.0009(2)	0	0	0.0004(2)
Cd11	$n = 1$	0	0	-0.0268(3)	0	0	-0.0024(3)
Cd12a	$n = 1$	0	0	0	-0.0070(2)	0.0111(2)	0.0044(3)
Cd12b	$n = 1$	0	0	0	0.0121(1)	0	-0.0245(3)

$$^a U_{\text{pos}}^{\mu}(\nu) = \sum_{n=1}^m S_n^{\mu} \sin(2\pi n\nu) + C_n^{\mu} \cos(2\pi n\nu).$$

Table 4. Occupational Modulation

atom	order	av occ.	occ. cos	occ. sin
Ce3a	$n = 1$	1/2	0.152(5)	-0.557(7)
Ce3b	$n = 1$	1/2	-0.320(5)	-0.509(5)
Ce4	$n = 1$	0.599(1)	-0.434(4)	0
Ce4	$n = 2$	1/2	-0.02(1)	0
Cd1a	$n = 1$	0.976(4)	0.031(4)	0.098(4)
Cd1b	$n = 1$	0.599	-0.017(5)	0.79(1)
Cd1b2	$n = 1$	0.401	0.016(5)	-0.79(1)
Cd1c	$n = 1$	0.401	-0.56(1)	-0.22(1)
Cd1c2	$n = 1$	0.599	0.55(1)	0.26(1)
Cd5a	$n = 1$	0.599	0.335(3)	0.456(3)
Cd5a2	$n = 1$	0.401	-0.315(3)	-0.470(3)
Cd5b	$n = 1$	1/2	0.015(4)	-0.609(6)
Cd5b	$n = 2$		0.04(1)	0.04(1)
Cd12a	$n = 1$	0.599	0.557(6)	0
Cd13	$n = 1$	0.401	0.434(4)	0
Cd13	$n = 2$		-0.02(1)	0
Cd14	$n = 1$	0.401	-0.425(7)	0.336(7)

by EDX (energy dispersive X-ray spectroscopy; detection limit for impurities ca. 0.1%) analysis using a JEOL JSM-820 SEM (scanning electron microscopy) system, operated at a 20 kV accelerating voltage with an Si detector using the system LINK AN 10000. Corrections were made for atomic number, absorption, and fluorescence using the ZAF method.

Single-Crystal X-ray Data Collection and Structural Refinement. The single-crystal X-ray diffraction data collection was performed for detailed structural analysis at ambient temperature on an Oxford Diffraction Xcalibur CCD diffractometer with graphite-monochromatized Mo K α radiation ($\lambda = 0.71073$ Å) operated at 50 kV and 40 mA with a detector to crystal distance of 80 mm. The intensities of the reflections were integrated using the

software supplied by the manufacturers of the diffractometer.^{21,22} Because of the irregular shape of the crystals, a numerical absorption correction, based on a shape obtained by optimizing the equivalence for symmetry related reflections, was performed with the programs X-RED²³ and X-SHAPE.²⁴ The structure was solved by direct methods using SHELXS-97,²⁵ and refinement was performed using the program JANA2000.²⁶ The structural drawings were rendered using the program Diamond, version 2.1c.²⁷ A detailed description of the crystal data, data acquisition, and refinements is given in Table 1.

Structural Solution

The satellite reflections clearly indicate a superstructure along the b^* -axis (in an orthorhombic setting). The crystal that yielded the strongest satellite reflections is metrically commensurate ($\mathbf{q} = 0 \ 2/3 \ 0$), and it may well be suspected to be in a lock-in phase. Other crystals tested yielded \mathbf{q} vectors in the range of $2/3$ – $3/4$, and these structures were

(21) Oxford Diffraction, *CrysAlis CCD*, p 171.31.2, 2006.

(22) Oxford Diffraction, *CrysAlis RED*, p 171.31.2, 2006.

(23) Computer code *X-RED*, version 1.07; Stoe and Cie GmbH: Darmstadt, Germany, 1996.

(24) Computer code *X-SHAPE*, version 1.01; Stoe and Cie GmbH: Darmstadt, Germany, 1996.

(25) Sheldrick, G.-M. *SHELXS-97: Program for the Solution of Crystal Structures*; University of Göttingen: Göttingen, Germany, 1997.

(26) Petříček, V.; Dušek, M.; Palatinus, L. *The Crystallographic Computing System JANA2000*; Institute of Physics AVCR: Praha, Czech Republic, 2000.

(27) Brandenburg, K. Computer code, *DIAMOND*, version 2.1c; Crystal Impac: Bonn, Germany, 1999.

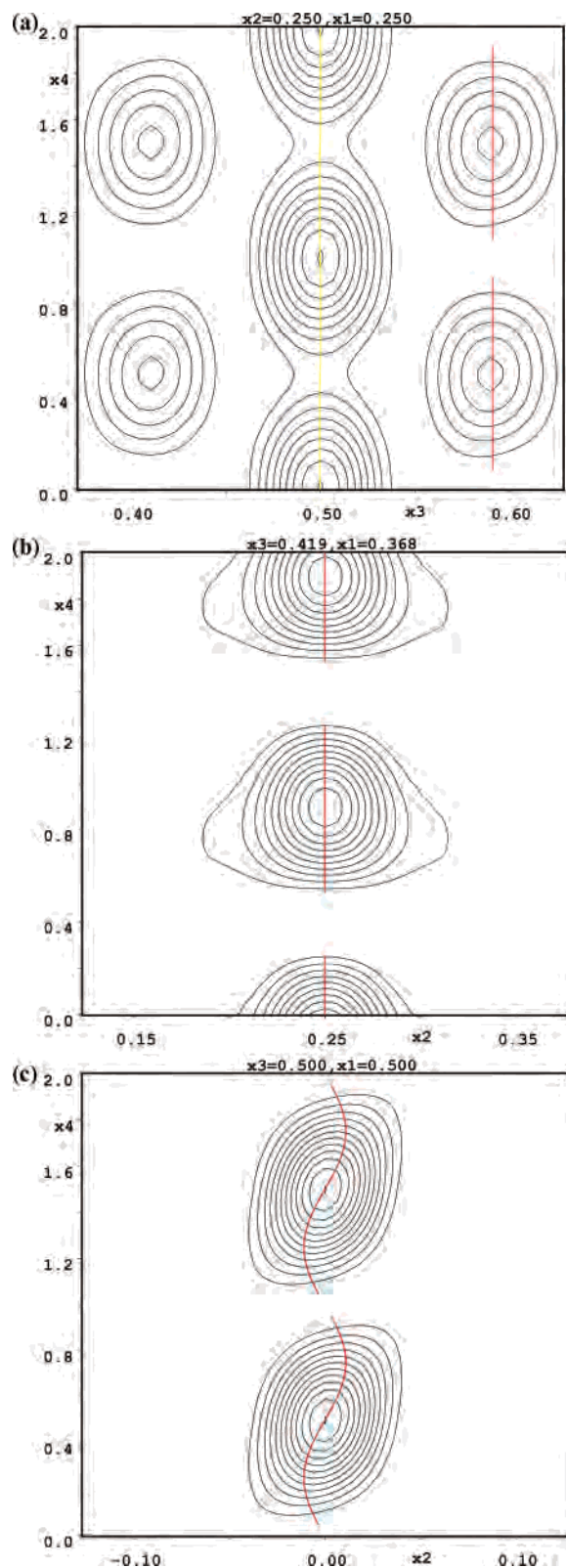


Figure 1. Electron density function of the modulated resolution of the disorder mechanisms. The locus of Ce atoms is given in yellow, and the locus of Cd is in red. The cutoff occupancy is 50%. The electron density variation is modeled by harmonic functions, and this leads to overlap for exchange functions. (a) Exchange mechanism I. The higher electron density of Ce4 forms the central feature along the internal space $\times 4$, while the Cd₂ (Cd13) pairs appear on either side. Note how the presence of density associated with the Cd₂ pair is correlated to the disappearance of the Ce4 atom. (b) Capping atom Cd14 (disorder mechanism II). (c) Cube center atom Cd12a (disorder mechanism III).

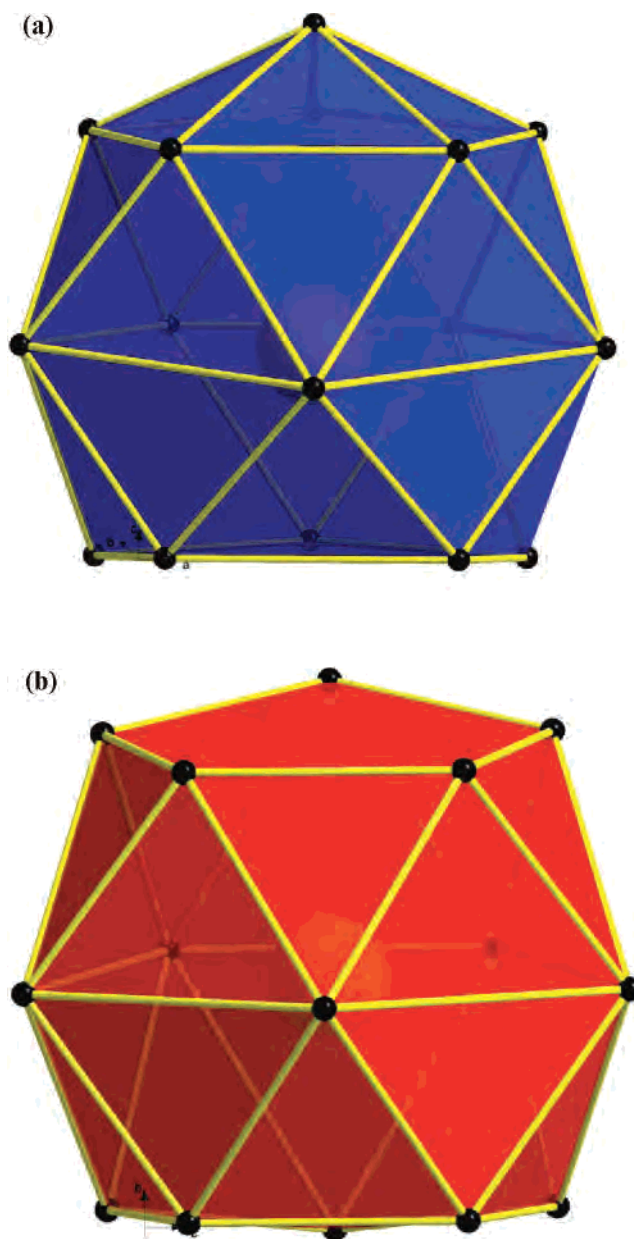


Figure 2. DPAPs surrounding the Ce positions Ce2 (a) capped and Ce1 (b) uncapped in the archetype structure Ce₁₃Cd₅₇.

refinable with the same modulated model, but due to the lower quality of data, the agreement was generally somewhat worse. This range is identical to that given in the Roof and Elliot paper.²⁰ Remarkably, no twinning was observed in the crystal. The unusual quality of this particular specimen is believed to be caused by the lock-in nature of the \mathbf{q} vector; this leads to more pronounced superstructure reflections and possibly to a more decisive violation of the hexagonal symmetry, which in turn makes twinning less probable. It is probable that both composition and annealing conditions contribute to this behavior. In view of the special extinction conditions (the hexagonal $hk0$ plane is void of any satellites) and the surrounding phase-field of a clearly incommensurate nature, it was, however, deemed useful to solve and refine the structure as a modulated phase. The satellite reflections were accordingly indexed using a fourth index, $hklm$, in

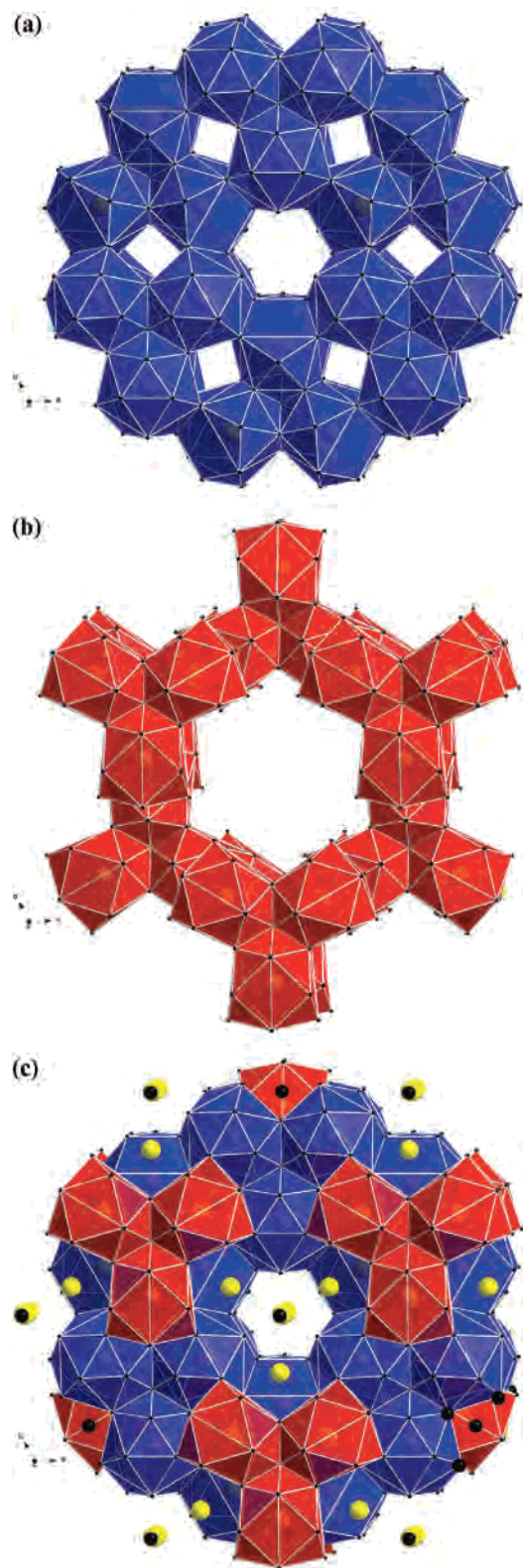


Figure 3. (a) Network formed by capped DPAPs surrounding Ce2 in the archetype structure $\text{Ce}_{13}\text{Zn}_{58}$. Note the presence of cubic interstices and the central, hexagonal channel. (b) Network formed by uncapped DPAPs surrounding Ce1 in the archetype structure $\text{Ce}_{13}\text{Zn}_{58}$. (c) Whole structure of the archetype $\text{Ce}_{13}\text{Zn}_{58}$. The only atomic positions not treated and engaged in the DPAP network are Zn12, which centers the cubes (hidden in this image, visible in Figure 2a), Zn11, and Ce4, which sits on the rotational hexad at the center of the tunnel, and Ce3, which sits at the center of this tunnel, effectively centering the pentagonal faces of the Ce2 DPAPs. Zn atoms are shown in black, and Ce atoms are in yellow.

addition to the conventional hkl of a normal crystal structure. The 3-D portion of the super space group was chosen as the highest allowed orthorhombic subgroup of $P6_3/mmc$, $Cmcm$. The modulation \mathbf{q} vector is parallel to b^* , and this is indicated by the second part of the superspace group symbol $(0\beta 0)$, and the extinction conditions for satellite reflections, indicated by their total absence in the hexagonal a^*b^* plane ($hk0m$; $m = 2n$ in orthorhombic setting), clearly show the presence of a glide component along the fourth dimension, associated with the reflection perpendicular to c , indicated by $00s$ in the super space group symbol. This symbol means that there are no translational components along the fourth, additional, dimension of the symmetry operations perpendicular to a and b but that there is a phase shift of π associated with the reflection perpendicular to c . Thus, the (maximal) super space group is $Cmcm(0\beta 0)00s$. All work on the structural solution was carried out using the software package JANA2000.²⁶ The basic structure was assumed to be an orthorhombic distortion of the archetype phase $\text{Ce}_{13}\text{Zn}_{58}$. After achieving convergence for the basic structure, the solution was inspected for signs of modulated behavior, and all the disorder mechanisms seen in previously solved structures²⁰ of the 13:58 phases were evident. These include disorder mechanism I, a pair exchange mechanism whereby the RE atom residing in the hexagonal channel (RE4) is partly exchanged for a Zn_2/Cd_2 dumbbell ($\text{Zn}_{13}/\text{Cd}_{13}$), disorder mechanism II, resulting in the inclusion of an interstitial Zn/Cd atom ($\text{Zn}_{14}/\text{Cd}_{14}$), and finally disorder mechanism III, partial occupancy of the interstitial positions in the Zn_8/Cd_8 cubes ($\text{Zn}_{12}/\text{Cd}_{12}$, described in Structural Description).

The origin of the modulated superstructure may well be assumed to be the resolution of some of the disordering mechanisms. To phase the satellite reflections, the positions corresponding to these occupational disorders were modeled with harmonic occupational modulations. In practice, this means that each position is modeled using not only the positional and thermal parameters of a normal structure but also a sinusoidal variation of the occupancy, whose period coincides with that defined by the \mathbf{q} vector. To start the refinement, each function is seeded by a very small, nonzero value. Allowing for occupational modulations led to an R value of 40% for the satellite reflections. While this is far from satisfactory, it provides starting phases for the satellites and allows for an inspection of the atomic positions surrounding the occupationally modulated positions. This gave a clear picture of the behavior of all positions. Importantly, all positions surrounding the occupationally modulated positions behaved as might be expected, with breathing motions, and subsequently, all other positions were modeled using first-order positional harmonics. While this improved the fit, it was clearly insufficient, leaving large residual electron densities, and second-order harmonics were introduced for some modulations. In the end, this also proved to be insufficient, and a few positions were modeled as partially ordered split positions. The final model is given in a nonconventional setting (origin shifted by $1/41/40$) of the super space group $Ccmm$ to make the atomic parameters

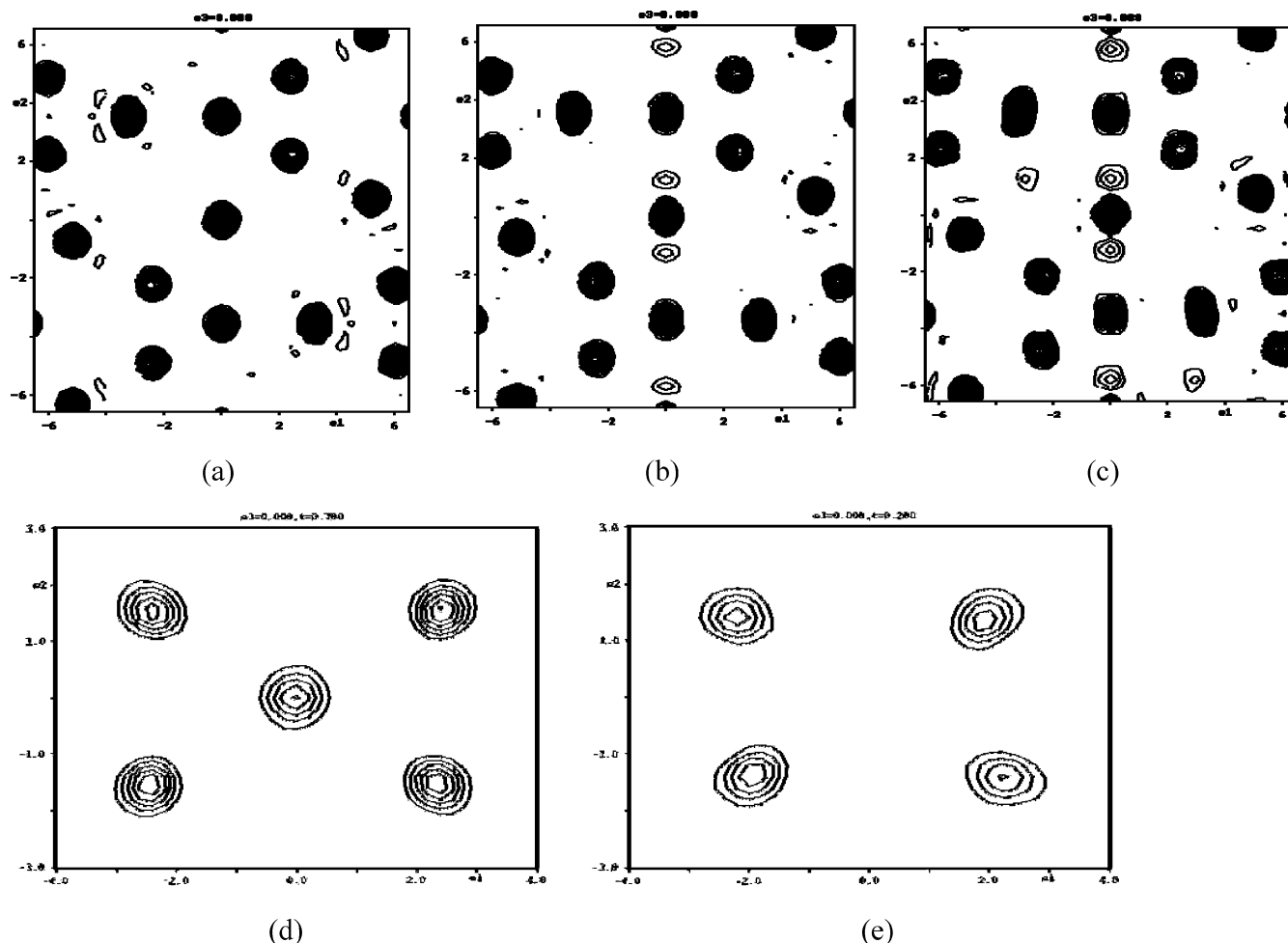


Figure 4. Three different disorder mechanisms shown in electron density maps. (a) $\text{Ce}_{13}\text{Zn}_{58}$ is fully ordered. (b) In $\text{Nd}_{12.82}\text{Zn}_{58.35}$, the atom Nd4 is partially replaced by a Zn2 dumbbell (Zn13) (i.e., disorder mechanism I). (c) For $\text{Sm}_{12.72}\text{Zn}_{59.08}$, an additional, partially occupied position occurs (Zn14). This is disorder mechanism II. The effect of this presence is clear from the elongated shape of the neighboring positions. Finally, panels d and e show the presence/absence of a Cd atom (Cd12a) in the cubic interstice in the structure of $\text{Ce}_{12.60}\text{Cd}_{58.68}$. This is disorder mechanism III. The relative positions of those different interstitials are evident in Figures 5 and 6.

directly comparable to the structures in the related systems. Refinement details are given in Table 1, parameters of the basic structure are given in Table 2, and modulation parameters are given in Tables 3 and 4. The refinement was carried out using a commensurate model, and this gave superior results as compared to an incommensurate approach. The electron density maps of positions corresponding to disorder mechanisms I–III are shown in Figure 1. An independent structural solution was carried out using charge flipping^{28–30} using the program Superflip,³¹ and the resulting structure was identical. Any suspicion of the modeling introducing structural prejudice can therefore be discarded.

Structural Description

The structure of the hexagonal archetype structure $\text{Ce}_{13}\text{Zn}_{58}$ has been described in some detail previously,¹⁹ and a

relatively short recap of the main structural features should suffice here. The structure consists of a number of local motifs, each associated with different order/disorder phenomena in the various superstructures encountered. The bulk of the structure is formed by double pentagonal anti-prisms (DPAP:s) of Zn surrounding Ce atoms (Figure 2). The DPAP:s surrounding the position Ce2 are essentially identical to those that build the cubic approximants. In those, the DPAP:s form superclusters of pseudo-icosahedral symmetry, but in hexagonal $\text{Ce}_{13}\text{Zn}_{58}$, they form a 6434 net that retains many of the local characteristics of the cubic phases, among these cubic Zn_8 interstices that are filled by a Zn atom in $\text{Ce}_{13}\text{Zn}_{58}$ (Figure 3a). A second set of uncapped DPAPs is formed around the position Ce1 (Figure 3b). These are sandwiched between layers of capped DPAPs (Figure 3c). A unique feature for the 13:58 type structures is a tunnel along the hexagonal axis that contains atoms unconnected to the DPAP:s (Figure 2). Three different local disordering schemes have been found in the $\text{RE}_{13}\text{Zn}_{58}$ systems. They include the partial replacement of an RE atom on the hexad by a pair of Zn atoms (disorder mechanism I), introduction of additional (Zn/Cd) capping atoms on the pentagonal faces

(28) Oszlanyi, G.; Suto, A. *Acta Crystallogr., Sect. A: Found. Crystallogr.* **2004**, *60*, 134.

(29) Oszlanyi, G.; Suto, A. *Acta Crystallogr., Sect. A: Found. Crystallogr.* **2005**, *61*, 147.

(30) Palatinus, L. *Acta Crystallogr., Sect. A: Found. Crystallogr.* **2004**, *60*, 604–610.

(31) Palatinus, L.; Chapuis, G. *J. Appl. Crystallogr.* **2007**, *40*, 786.

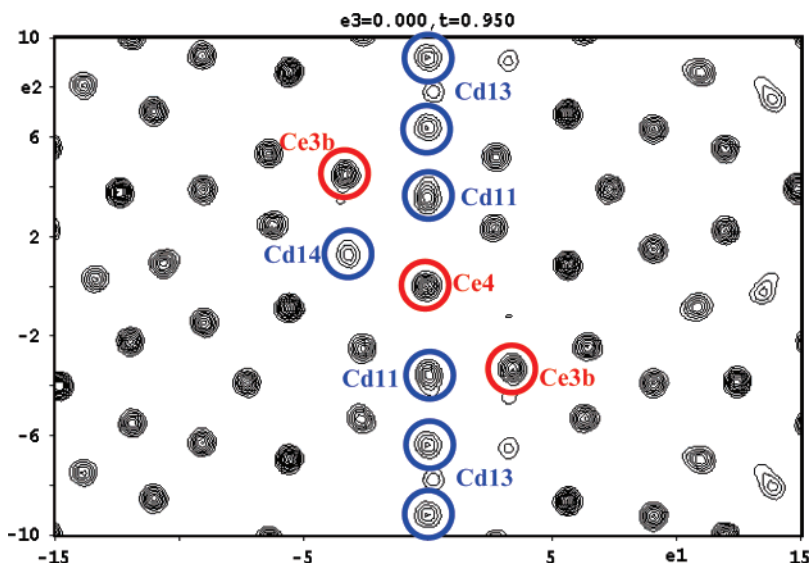


Figure 5. Projection of electron density maps from a 2 Å section of the [010] zone around Ce4. The axes are in angstroms, horizontal axis is a , vertical axis is c . The map is also a section through modulation space, generated for a τ -value of 0.95. Therefore, modulations are visible as static differences rather than as dynamic changes in electron density as in Figure 1. Note, however, the occupational modulation expressed in the presence of Ce4 and the concurrent absence of Cd13 in the center of the image. In the neighboring halfcells along c , the situation here is reversed, although the electron density of Ce4 here is nonzero due to a slight disorder. Note further the presence of Cd14, to the left of Ce4, and how Ce3 is displaced away from Cd14. The presence/absence of Cd14 correlates with the absence/presence of Cd13, but their out-of-phase behavior is only approximate.

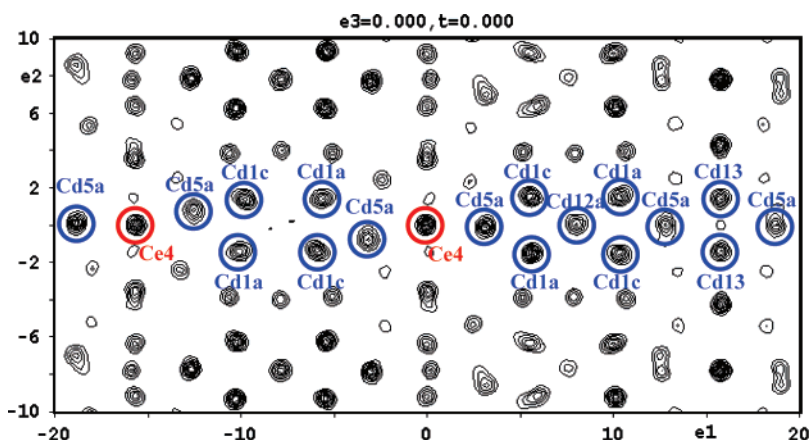


Figure 6. Projection of electron density maps from a 2 Å section of the $[1\bar{1}0]$ zone around Ce4. Horizontal direction is 110 and vertical is 001. The axes are labeled in angstroms. Relevant positions of Ce atoms are indicated in red, and Cd atoms are in blue. The simultaneous presence of Ce4 in neighboring subcells (left-hand side) leads to a crowding of the intermediate Cd atoms. The position of Cd5a is displaced away from the baseline, and the position corresponding to Cd12a becomes unoccupied. On the right-hand side, the position Cd12a is allowed since only one of the surrounding Ce4 positions is filled. Note how the Cd13 pair fits in the general packing scheme of the structure. Cd12a corresponds to a filled cubic interstice.

of the DPAP:s (disorder mechanism II), and partial occupancy of the Zn_8/Cd_8 cubes. Figure 4 depicts those three mechanisms in different systems. In some $RE_{13}Zn_{58}$ phases, the two later order/disorder mechanisms interact to yield a highly complex pattern of occupancy waves in the structure.³² For the Ho compound, the structure orders to give an incommensurately modulated phase where Zn atoms fill a sinusoidal tunnel in a manner similar to that of a composite structure. This behavior is also reminiscent of how the atoms in the cubic interstices interact with the disordered tetrahedra in the cubic approximant phases to yield disordered chains of atoms along the $\langle 111 \rangle$ directions of the cube. In $Ce_{12.60}-Cd_{58.68}$, we find, instead, an interplay between all three order/disorder mechanisms.

Starting from the Ce atom in the hexagonal channel (Ce4), and the pair exchange mechanism, this was modeled using a coupled harmonic function so that the presence of Ce excludes the simultaneous presence of a Cd_2 pair (Cd13). The occupancy of the Ce position refines to a value close to 0.6. From Figure 5, it is evident how the pair exchange mechanism couples to a displacement of the position Cd11 above and below the Ce/ Cd_2 entity, moving away from the Cd13 pairs. The capping atom Cd14 is also evident in this section, and the occupancy of this is coupled to the absence of the Cd_2 unit. The occupancy of Cd14 refines to close to 0.4, and in the final refinement, it was locked to a value complementary to that of Ce4. The capping atom Cd14 competes for space not only with Cd13 but also with Ce3b. Ce3b behaves like Cd11, moving out of the way of the sphere

(32) Piao, S. Y.; Lidin, S. *Inorg. Chem.* **2007**, *46*, 6452.

of influence from Cd14 into the next half cell along the hexagonal *c*-axis. The out-of-phase behavior of subsequent subcells along this direction ensures that this mechanism is viable.

The one remaining occupationally modulated position is that of Cd12a. This is the center of a Cd₈ cube. A sequence of electron density maps (Figure 6) again reveals the subtle interplay between occupancies and displacements. The presence of Ce4 causes short distances Cd5a–Ce4–Cd5a, and this leads to a buckling of the atomic chain Cd12a–Cd5a–Ce4–Cd5a–Cd12a and eventually to the expulsion of the position Cd12b. The cubic interstitial position empties. The emptying of this position on one side of the Ce4 leaves sufficient space to allow occupation of the Cd12a position. This concerted action also explains the somewhat puzzling sideways modulation motion of the position Ce4 (Table 3). The absence/presence of atoms surrounding the Ce4/Cd13 exchange pair leads to dramatic displacement modulations that are best modeled using split positions for these sites. For those atoms (Cd1b, Cd1b2 Cd1c, Cd1c2 Cd5a, Cd5a2, Cd12a, and Cd14), the relative occupancies were fixed to be the same as for the Ce4/Cd13 pair.

Conclusion

When the disorder mechanisms from previously known 13:58 phases interact, the resulting race-for-space yields a

very high degree of ordering. The crystal used in the final X-ray experiment was of unusual quality, showing no twinning, and strong satellite intensities. It may well be a lock-in phase, but a modulated description is still preferred, being more economical and yielding useful information also on other members of this family of intriguing structures. The behavior observed earlier for the interplay between the capping atom position Cd14 and the Cd₂ pair can be fully understood in light of this structure. In Tb₁₃Zn₅₉, full occupancy of the Zn14 position precludes any occupancy of the position corresponding to a Zn₂ pair, and in structures exhibiting both capping disorder and pair exchange disorder, the sum of the occupancies for these two positions always adds up to less than unity, allowing for exclusivity.

Acknowledgment. Financial support from the Swedish Natural Science Research Council and the Foundation for Strategic Research is gratefully acknowledged.

Supporting Information Available: CIF for Ce_{12.60}Cd_{58.68(2)}. This material is available free of charge via the Internet at <http://pubs.acs.org>.

IC701962B